Korean J. Chem. Eng., 32(5), 816-825 (2015)
DOI: 10.1007/s11814-014-0255-4

pISSN: 0256-1115
eISSN: 1975-7220

Turbulent flow and mixing performance of a novel six-blade grid disc impeller

Feng Ling Yang*,,†, Shen Jie Zhou*,**, and Cui Xun Zhang*****

*School of Mechanical Engineering, Shandong University, Jinan 250061, China
**Key Laboratory of High Efficiency and Clean Mechanical Manufacture (Shandong University), Ministry of Education, Jinan 250061, China
***Tianli Drying Equipment Incorporated Company, Shandong Province Academy of Sciences, Jinan 250014, China
(*Received 16 February 2014 • accepted 1 September 2014*)

Abstract−A novel six-blade grid disc impeller (RT-G) was designed and the single-phase turbulent flow and mixing in a baffled stirred tank agitated by this impeller were numerically studied by detached eddy simulation (DES) model. For comparison, a standard Rushton impeller (RT) with the same dimension was also investigated. The numerical results were compared with the reported experimental data and good agreements were obtained. Comparisons of the mean velocity, turbulent kinetic energy, power consumption and mixing time of RT and RT-G were performed. Results show that, for the tank stirred with RT-G, the velocity components can be increased in comparison with RT when the same power is consumed. The increase of the turbulent kinetic energy is about 20-30%. Besides, the mixing time for the tank stirred with RT-G is about 11% shorter than that of RT stirred tank operated at the same condition.

Keywords: Stirred Tank, Turbulence, Mixing, Power Consumption, Detached Eddy Simulation

INTRODUCTION

The stirred tank is one of the most widely used unit equipment in the chemical, pharmaceutical, biochemical, wastewater treatment and other industrial operations. However, its universality does not guarantee that we know much enough about the mixing processes occurring in it. Due to the complexity of the hydrodynamics in stirred tanks, mixing problems are usually addressed on a case-by-case basis. One of the main problems frequently encountered is how to improve the mixing efficiency.

Many investigations have been carried out to improve the performance of impellers and some efficient operation protocols have been developed, such as co-reverse periodic rotation and time-dependent fluctuation rotational speed protocols [1-5], eccentric impeller configuration protocols [6-10], and so on. All these investigations have proved to be profitable in increasing the mixing efficiency. However, while the mixing efficiency can be increased by these approaches, they are nevertheless of limited practical application because of the restriction of the motor and speed reducer about the co-reverse periodic rotation and time-dependent fluctuation rotational speed protocols, as well as low flexibility and reliability about the eccentric impeller configuration protocols [11].

In addition, different new types of impellers are continuously being developed [12-16]. We have designed a novel type of six-blade grid-disc impeller (referred to as RT-G). The objective was to investigate the turbulent flow and mixing performance of RT-G by using the computational fluid dynamics (CFD) method. The results were compared with those for RT to show its advantages in generating efficient flow and mixing in the stirred tank.

†To whom correspondence should be addressed.
E-mail: fly@sdu.edu.cn

Numerical predictions of the mixing process require an accurate presentation of the flow field. Previous studies have demonstrated that numerical simulations based on Reynolds-averaged Navier-Stokes (RANS) model can provide satisfactory results for the mean flow field in stirred tanks [17-19]. However, they invariably underpredict the turbulent kinetic energy, fail to capture the transient nature of the turbulent structures, and cannot account for the details of the vortices. This will certainly affect the predictions of the mixing time. Actually, the prediction of mixing time based on RANS model is usually two to three-times higher than that determined from experiments or empirical correlations reported in the literature [20-22]. To predict the turbulent quantities at small scales precisely, large eddy simulation (LES) or direct numerical simulation (DNS) is needed. However, LES and DNS both require expensive computational resources, and therefore cannot be used as a practical tool for the design of impellers. As an alternative, we adopted detached eddy simulation (DES) to investigate the turbulent flow and mixing in stirred tanks driven by RT and RT-G. This model combines the advantages of RANS and LES models, and can simulate the flow at less computational cost, as well as with high accuracy. Recent studies show that the DES model can also simulate the turbulent flow and mixing processes in stirred tanks. When performed on the same computational grid, which is under-resolved in the sense of LES, DES allows a better accuracy. Besides, it can provide improved predictions of the mean and turbulent quantities compared with those obtained by the RANS model [23-26].

The remainder of this paper is organized as follows: Section 2 describes the geometry and operating conditions of the stirred system. Section 3 presents the details of the numerical simulation processes and the numerical results are given in Section 4. Subsequently, utilizing these results, analysis and discussions of the flow features, mean velocity, turbulent kinetic energy, power consumption and mixing time are carried out. Finally, the conclusions of this work

are summarized in Section 5.

STIRRED TANK CONFIGURATIONS

As shown in Fig. 1, the stirred tank studied was a flat-bottomed cylindrical tank agitated by a Rushton turbine (RT) and a novel six-blade grid disc impeller (RT-G) proposed by the authors. Four full height baffles were provided at intervals of 90° against the wall of the tank. The dimensions of the stirred tanks are given in Table 1.

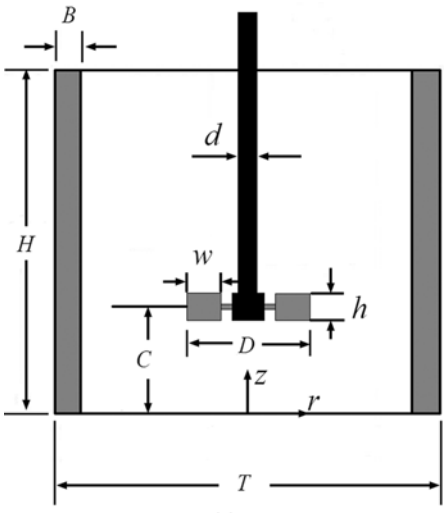

(a)

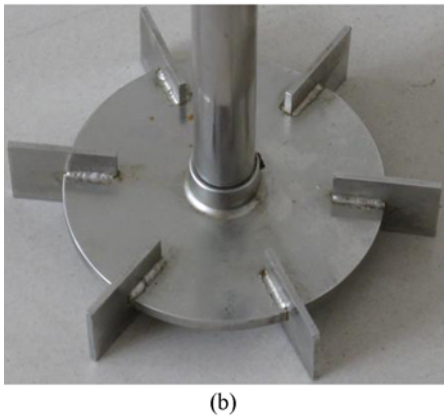

(b)

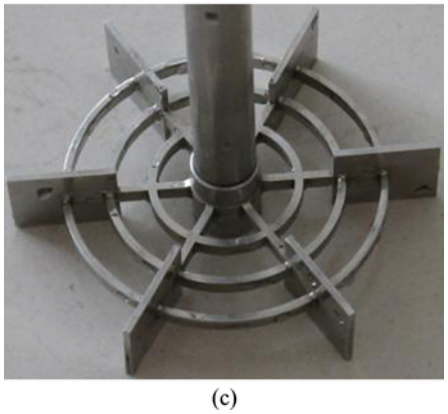

(c)

Fig. 1. Schematic diagram of the (a) stirred tank, (b) RT and (c) RT-G impeller investigated in this work.

Table 1. Dimensions of the stirred tank

Geometrical parameters (unit: mm)	RT	RT-G
Tank diameter (T)	147	147
Impeller shaft diameter (d)	8	8
Depth of liquid (H)	1 T	1 T
Impeller diameter (D)	T/3	T/3
Impeller clearance (C)	T/3	T/3
Impeller blade width (w)	D/4	D/4
Impeller blade height (h)	D/5	D/5
Impeller blade thickness (t_b)	1.5	1.5
Disc thickness (t_d)	1.5	1.5
Baffle width (B)	T/10	T/10
Baffle thickness (t_B)	T/100	T/100
Opening size (p)	/	3.5
Width of spoke (w_s)	/	1

Pure water with a density of $\rho=2\times10^3$ kg·m^{-3} and a dynamic viscosity of $\mu=0.001$ Pa·s was used as the working fluid. The rotational speed of the impeller was N=600 rpm (10 s^{-1}) in an anticlockwise direction as viewed from above, corresponding to an impeller tip speed $u_{tip}\approx1.54$ m·s^{-1} and a Reynolds number .

$$\mathrm{Re}=\frac{\rho \mathrm{ND}^2}{\mu}=2.4\times10^4.$$

NUMERICAL SIMULATION

1. DES Model

The turbulent fluid flow in the stirred tank is predicted by the DES model, which is formulated by replacing the distance function d in the one-equation Spalart-Allmaras (S-A) model with a modified distance function:

$$\tilde{\mathrm{d}}=\min\{\mathrm{d};\mathrm{C}_{\mathrm{DES}}\Delta\} \tag{1}$$

where $C_{DES}=0.65$ is the model empirical constant and Δ is the largest dimension of the grid cell in question. This modification of the S-A model changes the interpretation of the model substantially. In regions close to the wall, where $d<C_{DES}\Delta$, it behaves as a RANS model. Away from the wall, where $d>C_{DES}\Delta$, it behaves in a Smagorinsky-like manner and is changed to the LES model. The governing equation of DES model can be given as follows:

$$\frac{\partial\tilde{\nu}}{\partial t}+\langle u_i\rangle\frac{\partial\tilde{\nu}}{\partial x_i}=C_{b1}(1-f_{t2})\tilde{S}\tilde{\nu}+\frac{1}{\sigma}\left\{\frac{\partial}{\partial x_i}\left[(\nu+\tilde{\nu})\frac{\partial\tilde{\nu}}{\partial x_i}\right]+C_{b2}\left(\frac{\partial\tilde{\nu}}{\partial x_i}\right)^2\right\}-\left(C_{w1}f_w-\frac{C_{b1}}{c^2}f_{t2}\right)\left(\frac{\tilde{\nu}}{\tilde{d}}\right)^2 \tag{2}$$

The methodology proposed here has already been used in our previous work. For the purpose of simplicity, this is not given here. For more information, refer to Yang et al. [24-26].

2. Mixing Model

The mixing process can be predicted by introducing a virtual tracer and monitoring the concentration variations with time. In this section, DES computations were carried out to investigate the mixing processes of RT and RT-G. The mixing simulation was started

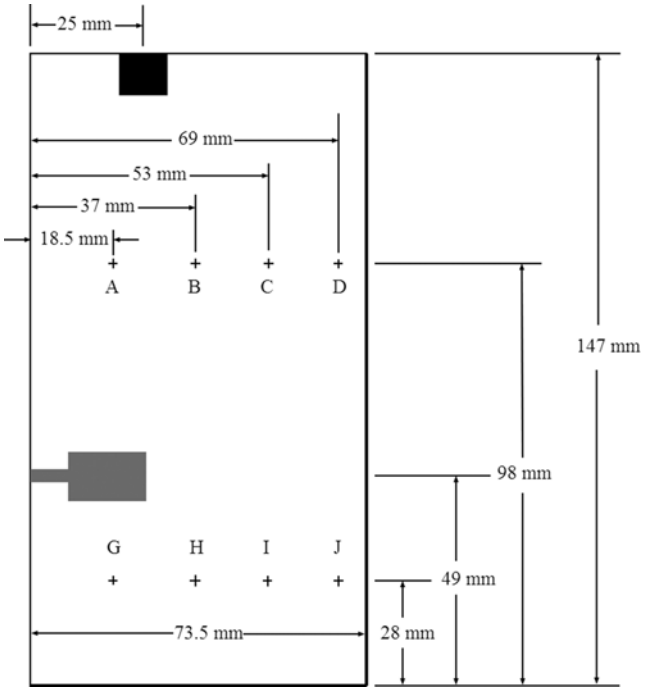

Fig. 2. Arrangements of the scalar tracer injection point (■) and the concentration monitoring points (+) in the θ=0° plane.

after a steady flow solution had been obtained. A total of 2.1 ml scalar tracer was added from the top surface at a location in the plane θ=0°. The distance from the tracer injection location to the axis of the stirred tank is 25 mm. The injection velocity was assumed to be the same as that of the local flow in the stirred tank, so that the tracer addition did not disturb the local flow structure. The concentration of the tracer was initialized as 1 in the feeding region, and in the rest region as 0. A total of eight monitoring points in the same plane were selected in regions of different agitation intensity, and the axial and radial positions are shown in Fig. 2.

In the simulation of a passive scalar transport, the instantaneous velocity affects the scalar evolution, while the passive scalar has no effect on the flow characteristics, so there is only one way interaction with the flow field. The scalar field is mathematically decoupled from the dynamical equations that govern the flow field and the solution of the scalar field. Therefore, a fully developed turbulent flow was used to solve the transient passive scalar transport equation.

The non-reacting mixing process was simulated by solving the scalar transport Eq. (3) to follow the transient concentration variations of the scalar tracer:

$$\frac{\partial(\rho\bar{c})}{\partial t}+\nabla\cdot(\rho\overline{\mathbf{u}c})=\nabla\cdot[(\Gamma_l+\Gamma_t)\mathrm{grad}(\rho\bar{c})]+S_c \quad (3)$$

where is the scalar variable, **u** is the velocity vector, S_c is the scalar source term, Γ_l is the molecular diffusivity of the scalar and Γ_t is the eddy diffusivity which is related to the eddy viscosity by the following relationship:

$$\Gamma_t=\frac{\mu_t}{\sigma_t} \quad (4)$$

where σ_t is the turbulent Schmidt number and is used to define the ratio of eddy viscosity to eddy diffusivity, which is in the range 0.7-0.9 depending on the type of flow. For the turbulent flow in stirred tanks, it was taken as 0.7 in the present study.

3. Computational Grid

Considering the unsteady nature of the flow, the whole stirred tank was modeled. The determination of the grid resolution is a critical point for numerical simulation. In the present work, the grids were prepared by the pre-processor Gambit 2.3 and a non-uniformly distributed hybrid unstructured mesh consist of about 490,000 cells was used for the calculation. Much attention had been given to locating more mesh points in the regions of high gradient around the blades and discharge region, where about 170,000 cells were employed. Along the impeller width, 25 nodes were assigned with the minimal grid length equals to 0.5 mm, which equals to about 0.01D. A similar grid resolution (970,997 cells for a stirred tank with a diameter T=0.3 m and Re=4.17×10^4) was employed by Zadghaffari et al. [27] in their LES study of the turbulent flow and mixing in a stirred tank driven by a Rushton turbine, and satisfactory results were obtained. The grids used here is also finer than the locally refined grid (0.023D) used by Revstedt et al. [28], who reported a good LES prediction of the turbulent flow. This implies that the grid resolution used in the present work is adequate to resolve the turbulent flow accurately.

4. Modeling Approach

The pressure-based Navier-Stokes algorithm was used for the solution of the model with implicit solver formulation where the absolute velocity formulation was adopted. To ensure smooth and better convergence, initially the k-ε computation was performed until a steady state flow field was obtained. Subsequently, the result of the steady-state computation was used as the initial solution to perform the unsteady DES computation. For modeling the impeller rotation, the multiple reference frame (MRF) method was used for the k-ε computation. Then it was switched to the fully transient sliding mesh (SM) method for the DES computation. In this method, the rotation of the impeller is explicitly taken into account and two fluid zones are defined: an inner rotating cylindrical volume centered on the impeller (rotor region) and an outer stationary zone containing the rest of the tank (stator region). In the present study, the boundary of the rotor region was positioned at r=0.0375 m and 0.034 m<z<0.064 m (where z is the axial distance from the bottom of the tank).

The initial condition for each simulation was that of still liquid. A flat liquid surface was assumed at the liquid surface by setting all the shear stress equal to zero. No-slip boundary condition was used at the impeller blades, the shaft and the tank walls. For the steady-state k-ε simulation, the standard wall functions were used to solve the near-wall flow. The SIMPLE algorithm was performed to couple velocities and pressure terms. The continuity equation, momentum conservation equation and k-ε equation were all discretized using the second-order upwind scheme to obtain a high-precision result. For the DES computation, The PISO discretization scheme was adopted to couple velocities and pressure terms. The PRESTO algorithm was adopted for the spatial discretization of the pressure item because it is optimized for swirling and rotating flow. The second order implicit scheme was used for time dis-

cretization. The bounded central differencing scheme was adopted for spatial discretization of momentum and the modified turbulent viscosity equation. This scheme blends the pure central differencing scheme with first- and second-order upwind schemes, and can reduce the unphysical oscillations in the solution field induced by the central differencing scheme. The energy conservation equation and concentration equation were all solved using the second order upwind scheme to obtain a high-precision result.

The time step and number of iterations are crucial to the transient DES modeling. The time step must be small enough to capture the flow features induced by the motion of the impeller. Furthermore, it also must be considered with the grid to ensure a stable and converged solution. In the present work, the simulations were performed with the time step $\Delta t=1\times10^{-4}$ s. Within each time step, a maximum of 40 iterations was performed so as to obtain the converged solutions quickly. The solution was considered to be fully converged when the normalized residuals of all variables were less than 1×10^{-4}. All the simulations were performed using the commercial CFD software Fluent 12.0 (Fluent Inc., USA) on a DEll T7500 workstation with two hex-core Xeon X5650 (2.67 GHz) processors and 32GB RAM in a parallel model.

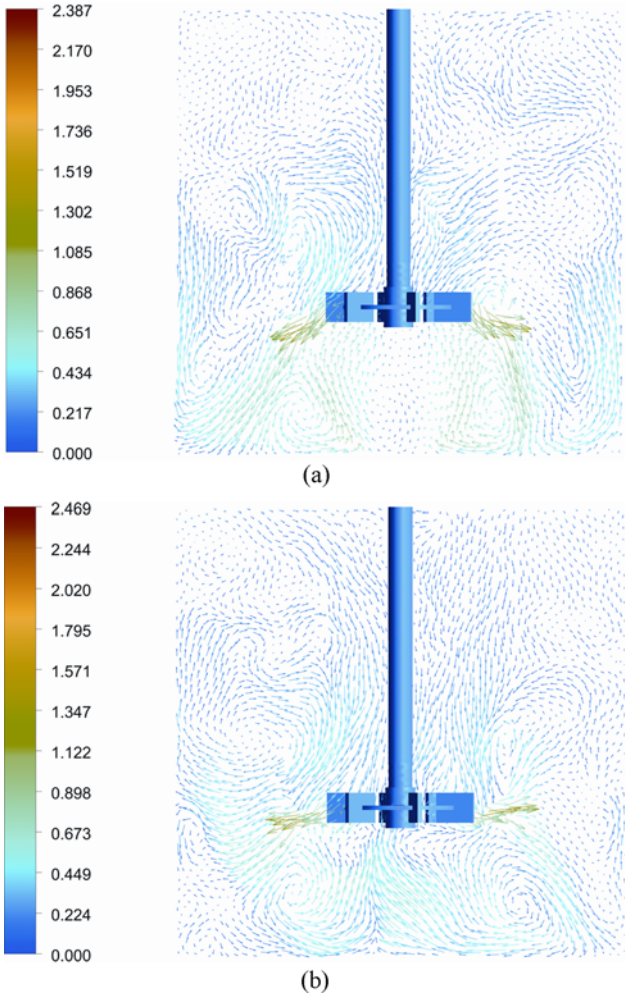

Fig. 3. Velocity vectors for the stirred tank agitated by (a) RT and (b) RT-G in the 0-180° plane at the time t=2 s.

RESULTS AND DISCUSSION

1. Flow Fields

The mixing performance of an impeller depends on the flow pattern generated in the stirred tank. Generally speaking, the more turbulent of the flow field, the faster the mixing can be completed. Here, we first compared the flow fields generated by RT and RT-G by comparing the flow features, mean velocity and turbulent kinetic energy profiles. Then, we pointed out the promising potential of RT-G for improving the mixing time and validate it in section 4.2.

1-1. Flow Features

Note that the flow field in the stirred tank is transient even after it is converged. For simplicity, here we only chose the velocity vectors at the time instant t=2 s (corresponding to 20 impeller revolutions) in the θ=0° plane for an example to clarify the differences of flow structures between RT and RT-G. The results are given in Fig. 3. Clealy, the fluid flow in the stirred tank is fully transient. Besides the large circulation loops, irregular secondary recirculation structures and many small vortexes of different scales are present throughout the tank. The flow fields generated by RT and RT-G are somewhat different. The most pronounced is that the axial flow capacity generated by RT-G is improved. Furthermore, differences between the velocity magnitudes are also apparent. The differences are partly due to intrinsic turbulent fluctuations, and partly due to the difference between the RT and RT-G configurations. Above analysis shows that a mixing performance improvement should be achieved by RT-G and this will be proved in section 4.2.

1-2. Mean Velocity Profiles

To do a quantitative analysis, mean velocity profiles in the vertical plane θ=0° of the stirred tank are given in Fig. 4. For comparison, the LDV results of Hockey [29] and the k-ε results of Javed et al. [30] are also presented. In these plots, the radial position r is normalized by the radius R of the stirred tank and the mean velocity is normalized by the blade tip velocity u_{tip}. Note that, although the dimensions of the stirred tank studied in this paper are different from that used by Javed et al. [30], geometrical similarity and fully turbulent flow conditions allow the direct comparison of the normalized velocity profiles [27].

In Fig. 4(a), the mean axial velocity u_z is depicted in the region near the liquid surface, as well as axial levels below and above the impeller. Good agreements between the DES and LDV results of the axial velocity generated by RT can be clearly observed from these plots, and thus, it can be said that applied methodology has yielded an acceptable agreement between experimental and simulated values, and accordingly, no experimental measurements of the velocity components generated by RT-G were performed. In addition, the axial velocities of the fluid in the tank stirred by RT-G are increased compared to those of the RT agitated tank, especially in the impeller discharge flow region. At the height of z/H=0.4, the maximum increase of the axial velocities is about 30%. The increase of the axial velocity components is not so much in the regions near the stirred tank bottom and the liquid surface. For example, at the height of z/H=0.8, the maximum increase of the axial velocities is no more 20%. It can be concluded that RT-G can improve the uniformity of the axial velocity distributions and strengthen the circulation of the fluid in the stirred tank.

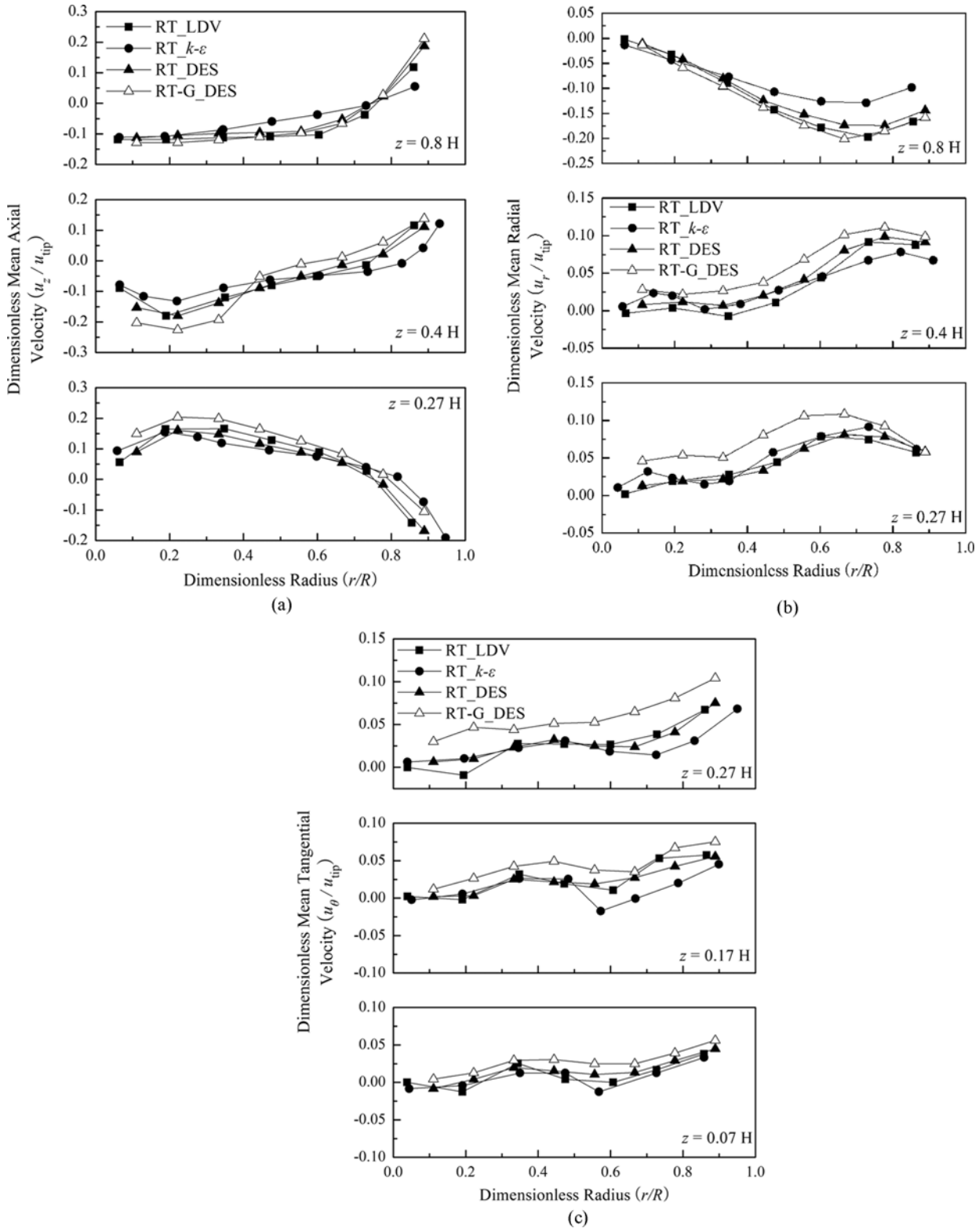

Fig. 4. Comparisons between the radial profiles of the mean (a) axial, (b) radial and (c) tangential velocity generated by RT and RT-G.

The radial velocity u_r is shown as radial profiles at seven axial levels in Fig. 4(b). Again, good agreement between the DES and LDV results has been achieved. By comparison, the radial velocities generated by RT-G have also been increased, though the increase is not so much than those of the axial components. The most noticeable increases can be found in the region above and below the impeller. In the region away from the impeller, only a little increase can be detected.

Fig. 4(c) reports radial profiles of the tangential velocity u_θ at three axial levels below the impeller. The prediction of tangential velocity cannot be evaluated in the regions above the impeller, as no experimental data in these regions were reported by Hockey [29]. It is evident that tangential velocity is small. However, relatively speaking, it is improved the most when compared with the other two velocity components, especially at the axial level of z/H=0.27, where a maximum increase of about three times can be detected.

1-3. Turbulent Kinetic Energy

To address why RT-G can increase the mean velocity components, the mixing mechanism was analyzed. It has already been confirmed that concentric stirred tank mixes only by virtue of perturbations generated by the periodic passing of impeller blades, which is responsible for the bulk convective mixing [31]. In this respect, RT and RT-G are equivalent in producing macro-mixing. Then, we can deduce there must be other reasons that cause the differences in the velocity profiles.

Besides the bulk convective motion, mixing in the stirred tank is also achieved by turbulent and molecular diffusion. In most cases, molecular diffusion is slow and it mainly contributes to the micro-mixing. Consequently, the probable reason may be the turbulent diffusion. Therefore, we analyzed the turbulent kinetic energy profiles in the whole stirred tank. In incompressible flows, the instantaneous quantity can be decomposed into three parts: a time average component, a deterministic periodic oscillation component, and a turbulent fluctuation component [32]. For the instantaneous velocity, it can be decomposed into the following three terms:

$$u_i = \overline{u}_i + \tilde{u}_i + u_i' \tag{5}$$

Accordingly, periodic and turbulent kinetic energy components can be determined. In Hockey [29], the turbulent kinetic energy was obtained from the experimentally measured fluctuating velocities. Following the same approach, the turbulent fluctuating component of the velocities was used to compute the turbulent kinetic energy by using the following expression:

$$k = \frac{1}{2}\sum_{i=1}^{3} u_i^{2} \quad (i = r, \theta, z) \tag{6}$$

The quantitative comparison between the turbulent kinetic energies generated by the RT and RT-G is shown in Fig. 5. Clealy, the turbulent fluctuations in the tank stirred by RT-G are more intense than that in the tank stirred by RT. In the regions above and below the impeller, an average increase of nearly 30% can be observed. Away from the impeller, the average increase is relatively low, but it is still about 20%. Such increases may be attributed to the fact that, in the stirred tank agitated by RT-G, the fluid above and below the impeller can directly exchange with each other. This will inevitably modify the turbulence structures and result in much more small-scale vortices in the impeller region. Simultaneously, these small-scale vortices are spread to other regions in the stirred tank by bulk convective mixing and certainly affect the profiles of the turbulent kinetic energies.

2. Mixing Characteristics

2-1. General Mixing Pattern

The simulated 2D contour plots of the scalar concentration in the (r−z) vertical planes at 0° and 180° angular positions, which

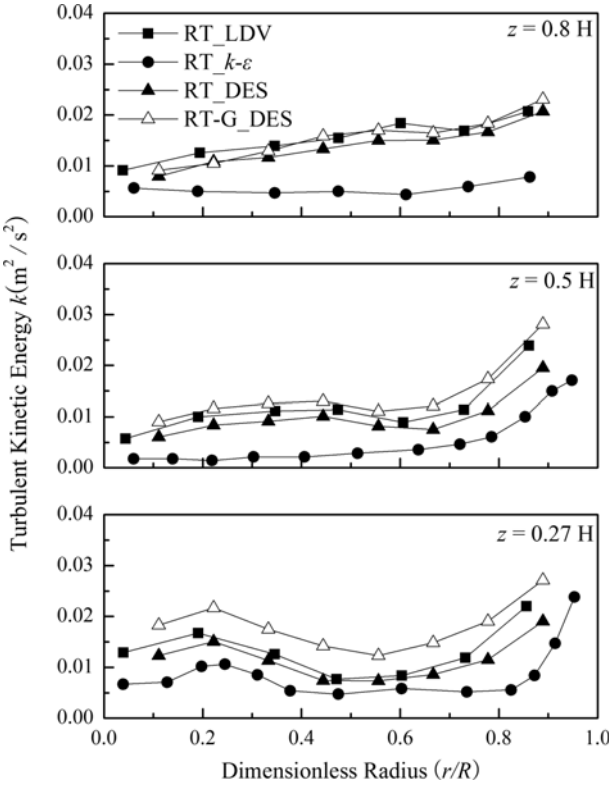

Fig. 5. Comparisons between the radial profiles of turbulent kinetic energy generated by RT and RT-G.

clearly express the scalar concentration evolution in the tank, are shown in Fig. 6 and 7. It is apparent that the DES model can provide detailed spatial and temporal evolution of the scalar concentration and accordingly give the mixing characteristics during the mixing stages at various positions. Overall, the mixing patterns of RT and RT-G are similar. After injection, the tracer is transported in the tangential direction near the top surface of the liquid and also in the axial direction towards the impeller. When the tracer reaches the impeller, it is transported towards the tank wall by the impeller stream. Then the tracer splits upwards and downwards along the wall. With progress in time, the tracer moves towards the top liquid surface as well as the bottom of the tank. The tracer is then convected back towards the impeller by the recirculating flows in the upper and lower parts of the tank. Finally, the tracer concentration field approaches a uniform distribution after about 3.0 s. The predicted evolution of the tracer concentration field in the tank resembles qualitatively that observed using high-speed video visualization by Togatorop and Mann [33] and the k-ε predictions of Javed et al. [30]. However, the k-ε predicted concentration field is symmetrical, while the DES predicted tracer concentration field is asymmetrical, indicating that DES model can capture the transient mixing process in the stirred tank. Besides, in the tank agitated by RT-G, a faster mixing process can be achieved than the RT agitated tank. This finding shows that RT-G can give better mixing performance than RT.

2-2. Mixing Time

Mixing times can be determined based on the tracer concentration variation curves using the conventional 95% ruler, which is

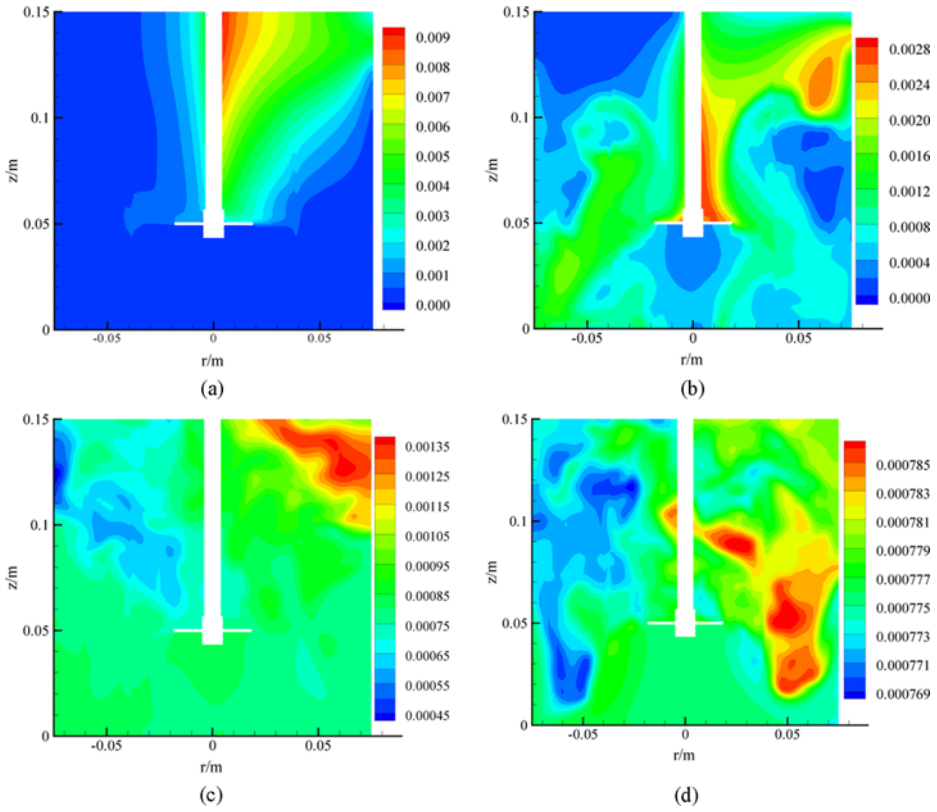

Fig. 6. DES predicted tracer concentration distributions of RT as a function of time in the r-z vertical plane: (a) 0.3, (b) 1, (c) 2 and (d) 4 s after injection of the scalar tracer.

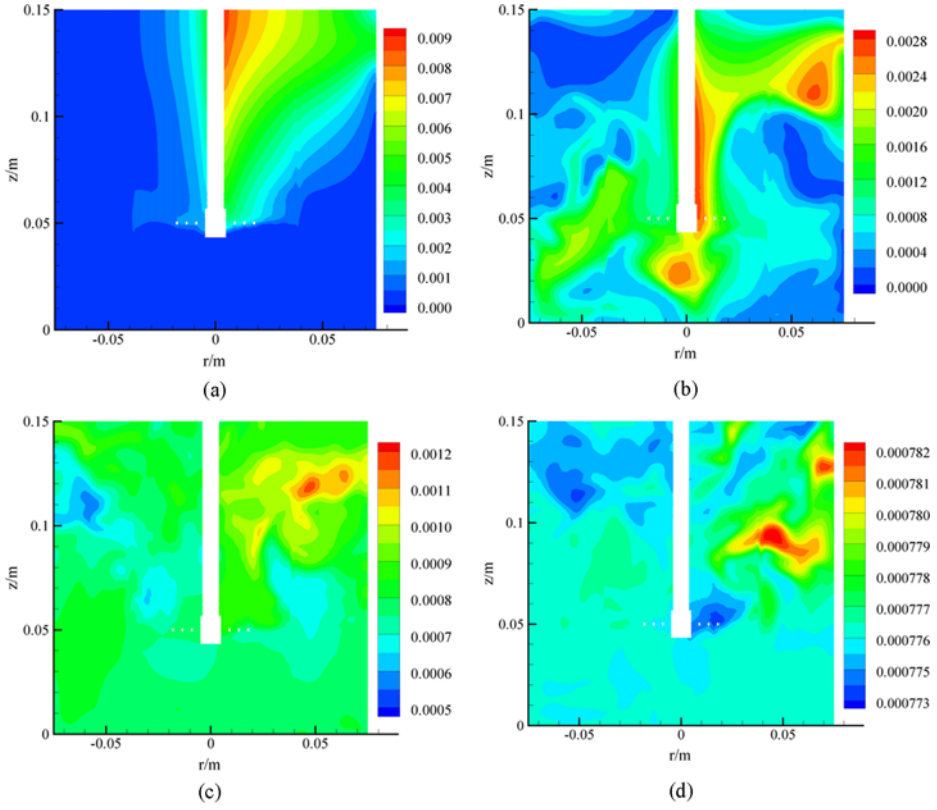

Fig. 7. DES predicted tracer concentration distributions of RT-G as a function of time in the r-z vertical plane. Same conditions as in Fig. 6.

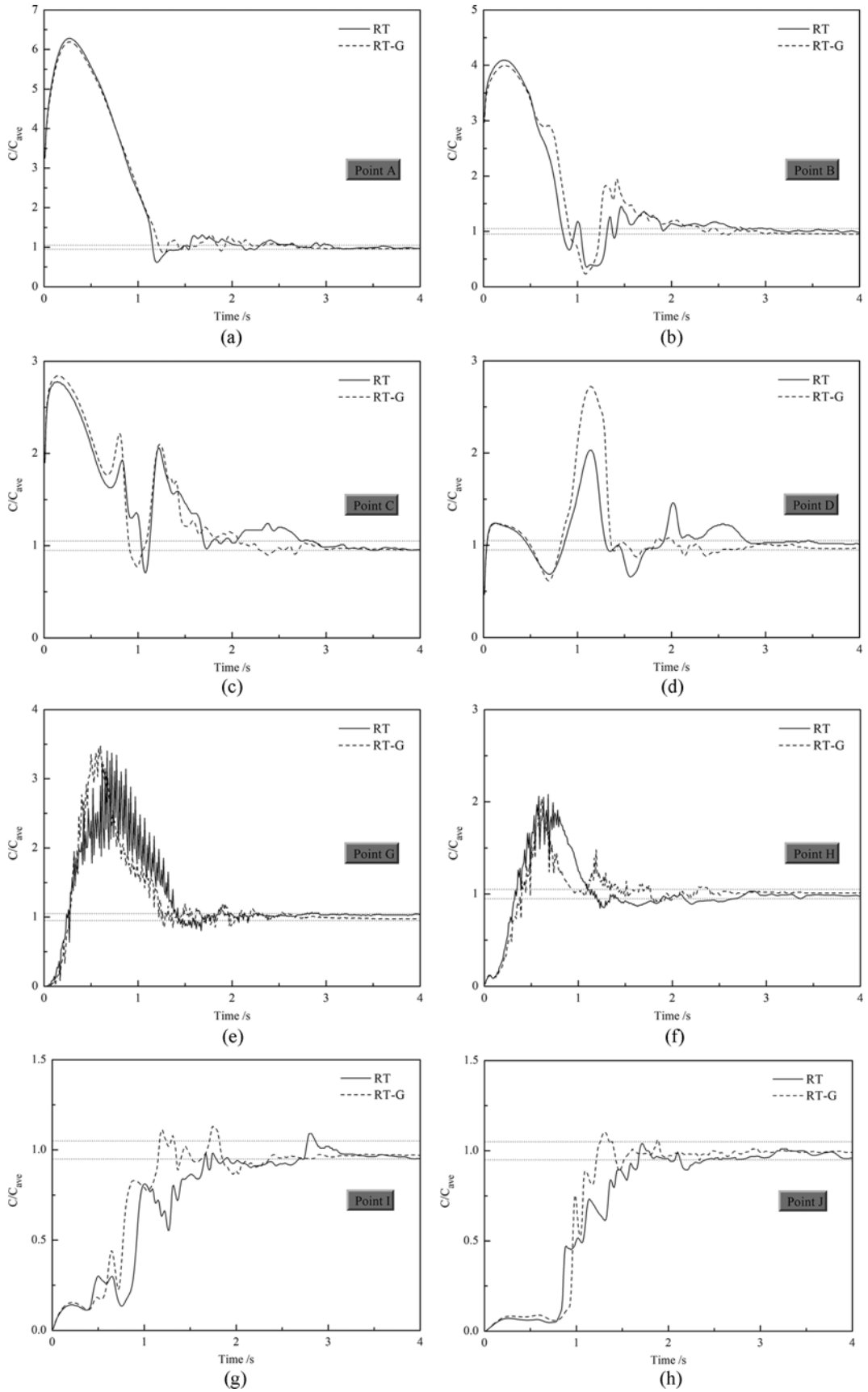

Fig. 8. Time variations of the tracer concentrations for the stirred tank agitated by RT and RT-G at different positions in the θ=0° plane: (a) point A, (b) point B, (c) point C, (d) point D, (e) point G, (f) point H, (g) point I, (h) point J.

Table 2. Mixing times of RT and RT-G

Monitoring points	Mixing time, t_{95} (s)			
	RT			RT-G
	k-ε	Experimental	DES	DES
A	3.1	3.1	3.1	2.7
B	2.8	3.5	3.0	2.8
C	2.2	3.0	2.8	2.7
D	2.9	3.0	2.8	2.5
G	2.9	3.6	2.9	2.5
H	2.7	2.8	2.7	2.4
I	2.5	3.6	2.9	2.4
J	2.4	2.5	2.4	2.3
Average	2.7	3.1	2.8	2.5

the time required for the tracer concentration to reach ±5% of the final equilibrium value. Typical variations of the tracer concentration with time at the selected monitoring points in the stirred tank are shown in Fig. 8. In these plots, the tracer concentration was normalized by the fully mixed value and the mixing time was denoted as t_{95}. No matter RT or RT-G, there are both large fluctuations of the tracer concentration in the initial stages of mixing. Then it approaches the equilibrium value asymptotically. However, the time needed for RT and RT-G to approach the final equilibrium value is different, and this can be confirmed by the DES predicted mixing times listed in Table 2. No mixing time experiment was conducted here and the numerical results were compared with the experimental data from literature. For comparison purposes, the k-ε predictions and the experimental results of RT cited from the literature of Javed et al. [30] and Distelhoff et al. [34] are also listed. Generally, the DES predicted mixing times of RT compare well, with an under-prediction within 20%, with the values measured by PLIF experiments. By comparison, the k-ε predictions are not so good. From Table 2, the mixing time is a local variable, which depends on the positions of the monitoring points. By contrast, variations of the mixing times for RT-G at different monitoring points are small, which shows that RT-G can improve the mixing uniformity and has better mixing performance than RT. Besides, the average mixing time of RT-G is about 11% shorter than that of RT determined at the same condition. The magnitude of the difference between the local mixing times of the two impellers varies with positions. The biggest difference is up to 17.5%, which is found in the impeller discharge flow region, indicating that RT-G is more efficient.

3. Power Consumption

Power consumption is a very important parameter which contributes significantly to the overall operation costs of a stirred tank. It is defined as the amount of energy necessary in a period of time to generate the movement of the fluid within the tank by means of mechanical agitation [35]. A stirred tank in which the mixing process can be performed efficiently with the lowest mixing time and with the minimum energy is the most highly desired.

There are many devices that can be used to measure the power consumption in stirred tanks, such as wattmeter, ammeter, calorimeter, dynamometer, torquemeter and systems based on strain gauges. The principles of these systems and their characteristics are reviewed by Ascanio et al. [35]. In the present work, we measured the power consumption with a torque transducer mounted on the impeller shaft. It can be adapted for real-time measurements of the torque, impeller rotational speed and power consumption. It is worth noting that the power consumed by the motor, bearing box, as well as the energy losses due to friction, must be taken into account when computing the power consumed by the fluid. Therefore, the power consumptions with and without load were respectively measured and the difference between them is the actual power consumption.

The non-dimensional power number is commonly used to evaluate the efficiency of stirred tanks:

$$N_p = \frac{P}{\rho N^3 D^5} \tag{7}$$

where P is the power consumption, which can be calculated as the angular velocity times the torque acting on impeller blades and shaft [36]:

$$P = \omega \cdot M = \omega \cdot \int_A \mathbf{r} \times \boldsymbol{\tau} \cdot d\mathbf{A} \tag{8}$$

where ω is the angular velocity vector, M is the torque, A is the surface of the impeller and shaft, $\mathbf{r}$ is the position vector, $\boldsymbol{\tau}$ is the stress tensor, and d$\mathbf{A}$ is the differential surface vector. The procedure of power estimation directly from a calculation of the total torque required to rotate the shaft and impeller is reliable because the flow field around the impeller is resolved. It is not necessary to calculate the viscous energy dissipation term from the calculated velocity field and accordingly, reduces the computational time requirement [37].

The simulated and experimentally measured power numbers of RT and RT-G are compared in Table 3. From a quantitative comparison, the simulated power numbers of RT and RT-G are in good agreement with the experimental values with an under-prediction within 10%. For RT, the experimentally determined power number is 5.42, which is consistent with the result reported by Rutherford et al. [38]. By comparison, the power number of RT-G is about 1.3% lower than the counterpart of RT. The difference is negligible and we can conclude that the power consumptions of RT and RT-G under the same operating conditions are identical.

CONCLUSIONS

The turbulent flow and mixing in a tank stirred by RT-G was studied using the DES model. The sliding mesh approach was employed to simulate the rotation of the impeller. Computations of the mean velocity components, turbulent kinetic energy, power con-

Table 3. Power numbers of RT and RT-G

Impeller	Experimental result	Numerical result	Δ (%)[a]
RT	5.42	4.94	−8.86
RT-G	5.35	4.86	−9.16

[a]Difference between the simulated and experimentally measured values

sumption and mixing time were conducted. The results were compared with those of RT and good improvements were observed. Specifically, the axial velocities can be increased about 20% compared with those in the tank stirred by RT. The increase of radial velocities is not so much and the tangential component is the least affected except in the region near the impeller. RT-G can also improve the turbulent kinetic energy and can achieve homogeneous mixing status faster than RT under the same operating condition with the same power consumption.

Finally, the effects of the impeller rotational speed, impeller diameter, and grid opening size should further investigated to evaluate the hydrodynamics and mixing performance of RT-G. In addition, an optimized design of the configuration of RT-G and its application in the gas-liquid mixing, especially the gas dispersion performance in the region adjacent to the impeller, should also be carried out.

ACKNOWLEDGEMENTS

Financial support from NSFC (National Natural Science Foundation of China) (No. 21306105) is gratefully acknowledged.

REFERENCES

1. M. Kordas, G. Story, M. Konopacki and R. Rakoczy, *Ind. Eng. Chem. Res.*, **52**, 13818 (2013).
2. D. J. Lamberto, F. J. Muzzio and P. D. Swanson, *Chem. Eng. Sci.*, **51**, 733 (1996).
3. S. Roy and S. Acharya, *Chem. Eng. Res. Des.*, **90**, 884 (2012).
4. W. G. Yao, H. Sato, K. Takahashi and K. Koyama, *Chem. Eng. Sci.*, **53**, 3031 (1998).
5. M. Yoshida, M. Shigeyama, T. Hiura, K. Yamagiwa, A. Ohkawa and S. Tezura, *Chem. Eng. Commun.*, **194**, 1229 (2007).
6. D. Bulnes-Abundis and M. M. Alvarez, *AIChE J.*, **59**, 3092 (2013).
7. A. Hidalgo-Millán, E. Soto, R. Zenit and G. Ascanio, *Can. J. Chem. Eng.*, **89**, 1051 (2011).
8. J. Karcz, M. Cudak and J. Szoplik, *Chem. Eng. Sci.*, **60**, 2369 (2005).
9. G. Montante, A. Bakker, A. Paglianti and F. Magelli, *Chem. Eng. Sci.*, **61**, 2807 (2006).
10. S. Woziwodzki, L. Broniarz-Press and M. Ochowiak, *Chem. Eng. Res. Des.*, **88**, 1607 (2010).
11. K. Takahashi, *J. Chem. Eng. Jpn.*, **40**, 605 (2007).
12. V. Buwa, A. Dewan, A. F. Nassar and F. Durst, *Chem. Eng. Sci.*, **61**, 2815 (2006).
13. M. Campolo, A. Paglianti and A. Soldati, *Ind. Eng. Chem. Res.*, **41**, 164 (2002).
14. N. J. Fentiman, N. St. Hill, K. C. Lee, G. R. Paul and M. Yianneskis, *Chem. Eng. Res. Des.*, **76**, 835 (1998).
15. Z. H. Liu, X. Y. Yang, Z. M. Xie, R. L. Liu, C. Y. Tao and Y. D. Wang, *CIESC J.*, **64**, 2794 (2013).
16. E. S. Szalai, P. Arratia, K. Johnson and F. J. Muzzio, *Chem. Eng. Sci.*, **59**, 3793 (2004).
17. A. Brucato, M. Ciofalo, F. Grisafi and G. Micale, *Chem. Eng. Sci.*, **53**, 3653 (1998).
18. M. Jenne and M. Reuss, *Chem. Eng. Sci.*, **54**, 3921 (1999).
19. B. N. Murthy and J. B. Joshi, *Chem. Eng. Sci.*, **63**, 5468 (2008).
20. W. Bujalski, Z. Jaworski and A. W. Nienow, *Chem. Eng. Res. Des.*, **80**, 97 (2002).
21. Z. Jaworski, W. Bujalski, N. Otomo and A. W. Nienow, *Chem. Eng. Res. Des.*, **78**, 327 (2000).
22. J. J. Osman and J. Varley, *IChemE Symp. Ser.*, **146**, 15 (1999).
23. J. Gimbun, C. D. Rielly, Z. K. Nagy and J. J. Derksen, *AIChE J.*, **58**, 3224 (2012).
24. F. L. Yang, S. J. Zhou and G. C. Wang, *Comput. Fluids*, **64**, 74 (2012).
25. F. L. Yang, S. J. Zhou, C. X. Zhang, G. M. Evans and G. C. Wang, *Chem. Eng. Commun.*, **200**, 1347 (2013).
26. F. L. Yang, S. J. Zhou, C. X. Zhang and G. C. Wang, *Korean J. Chem. Eng.*, **30**, 1843 (2013).
27. R. Zadghaffari, J. S. Moghaddas and J. Revstedt, *Comput. Fluids*, **39**, 1183 (2010).
28. J. Revstedt, L. Fuchs and C. Trägårdh, *Chem. Eng. Sci.*, **53**, 4041 (1998).
29. R. M. Hockey, Ph.D. Thesis, Imperial College, London (1990).
30. K. H. Javed, T. Mahmud and J. M. Zhu, *Chem. Eng. Process.*, **45**, 99 (2006).
31. M. M. Alvarez, T. Shinbrot, J. Zalc and F. J. Muzzio, *Chem. Eng. Sci.*, **57**, 3749 (2002).
32. A. Delafosse, A. Line, J. Morchain and P. Guiraud, *Chem. Eng. Res. Des.*, **86**, 1322 (2008).
33. A. Togatorop and R. Mann, *AIChE Symp. Ser.*, **90**, 19 (1994).
34. M. F. W. Distelhoff, A. J. Marquis, J. M. Nouri and J. H. Whitelaw, *Can. J. Chem. Eng.*, **75**, 641 (1997).
35. G. Ascanio, B. Castro and E. Galindo, *Chem. Eng. Res. Des.*, **82**, 1282 (2004).
36. A. D. Harvey and S. E. Rogers, *AIChE J.*, **42**, 2701 (1996).
37. S. S. Murthy and S. Jayanti, *Chem. Eng. Res. Des.*, **80**, 482 (2002).
38. K. Rutherford, K. C. Lee, S. M. S. Mahmoudi and M. Yianneskis, *AIChE J.*, **42**, 332 (1996).